optica

Surface plasmon laser with two hole arrays as cavity mirrors

E. W. DE VOS, M. J. A. DE DOOD, [ID] AND M. P. VAN EXTER* [ID]

Huygens-Kamerlingh Onnes Laboratory, Leiden University, P.O. Box 9504, 2300 RA Leiden, The Netherlands
Corresponding author: exter@physics.leidenuniv.nl

Surface plasmon propagation and scattering on structured metal–dielectric interfaces are important tools for field confinement and enhanced atom–field interaction. In this paper, we demonstrate a new type of surface plasmon (SP) lasing that more closely resembles the usual mirror-based laser, in a geometry that comprises a central 50-µm-long flat region between two metal hole arrays that serve as reflecting mirrors. The lasing mode shows features of double-slit interference modulated by the radiation pattern of, and selection rules set by, the scattering of SPs on the 2D hole arrays. Our results also provide information on the group velocity of surface plasmons and their scattering and penetration in hole arrays.   © 2019
Optical Society of America under the terms of the OSA Open Access Publishing Agreement

https://doi.org/10.1364/OPTICA.6.000092

Surface plasmons can be described as electromagnetic surface waves propagating along a conducting surface or thin film [1]. Their localization and field-enhancing properties make them ideally suited for applications in biosensing [2–5], nanophotonics [6–8], integrated optical circuits [9,10], and other areas benefiting from strong atom–field interaction and field confinement [11,12].

In recent years, the introduction of semiconductor and dye gain media has allowed for the compensation of ohmic losses [13,14] and the use of surface plasmon lasing as a means of studying the properties of SPs [15,16]. By combining loss compensation with the structuring of metals on a nanometer size scale, SP lasing has been accomplished in geometries including metal-coated nanocavities [17,18] and nanopillars [19], hybrid plasmonic waveguides [20], and metal hole arrays [15].

In this Letter, we use a Fabry–Perot cavity geometry, where metal hole arrays act as distributed Bragg reflectors (DBRs) and the backscattering of SPs between the two arrays results in coherent lasing emission. We extract important quantities, such as the group velocity and relevant scattering rates on subwavelength size holes, via a simple method that is applicable to any metal–semiconductor interface that supports surface plasmons.

We study surface plasmons at an interface of gold and an actively pumped semiconductor. The layer structure of our sample comprises a 100-nm-thick gold layer on a 150-nm-thick In$_{0.53}$Ga$_{0.47}$As layer, which is lattice matched to an InP substrate. During the growth, a 10–15 nm thin InP spacer layer followed by ≈ 5 nm SiN$_x$ is inserted between the In$_{0.53}$Ga$_{0.47}$As and the metal. A 0.5 nm Cr sticking layer is used for adhesion of the gold to the SiN$_x$. A 20-nm-thick Cr layer on top damps the surface plasmons on the gold–air interface.

Several square hole arrays with a lattice constant of $a_0 = 450$ nm ($\approx$ SP wavelength) were patterned into the gold layer with a nanolithographic method that produces holes with a diameter of $d \approx 200$ nm (see [21] for more details on the production process). A different e-beam dose was chosen for each array, leading to different hole sizes (≈ 20 nm variation in diameter). All arrays are 50 µm × 50 µm and are separated by patches of 50 µm of unpatterned gold. In this Letter, we will study the properties of SPs traveling back and forth between two hole arrays.

The In$_{0.53}$Ga$_{0.47}$As layer is optically excited through the substrate by a Nd:YAG laser of wavelength 1064 nm, with an approximately elliptically shaped pump spot with a 40 × 50 µm FWHM axis at the sample (long axis connecting the two arrays). The sample is cooled to 100 K in a helium flow cryostat.

The light emitted by the device is collected in transmission on the air side with a 20 × microscope objective (N.A. = 0.4) combined with a $f = 200$ mm tube lens to produce a 20 × direct image. By adding an extra lens, we can, alternatively, produce a far-field (angle-resolved) image of the emission. We observe these emission patterns in two ways: either directly with a InGaAs CCD (Xenics Xeva 1.7-320) or by scanning a multimode fiber (62.5 µm core) through the detection plane. The light incident on the CCD is spectrally filtered with two long-pass filters (cutoff wavelengths 1000 nm and 1100 nm), to remove the 1064 nm pump beam and ambient light, and a Gaussian bandpass filter ($\lambda_c = 1480$ nm, FWHM = 12 nm) to select part of the emission and lasing spectrum of the device. The role of the 1000 nm filter is to remove a small fraction of the ambient light that could still pass through the 1100 nm filter, because this filter was less ideal than we had hoped it would be. The light collected by the fiber is analyzed with a grating spectrometer to enable simultaneous spectral and spatial imaging.

With the excitation spot positioned between two hole arrays, we observe optical emission at the edges of the arrays. The emitted power shows a clear lasing threshold around $P_{in} \approx 230$ mW [see inset of Fig. 1(a)], slightly larger than the threshold for individually pumped arrays, which was found to be $P_{in} \approx 200$ mW with
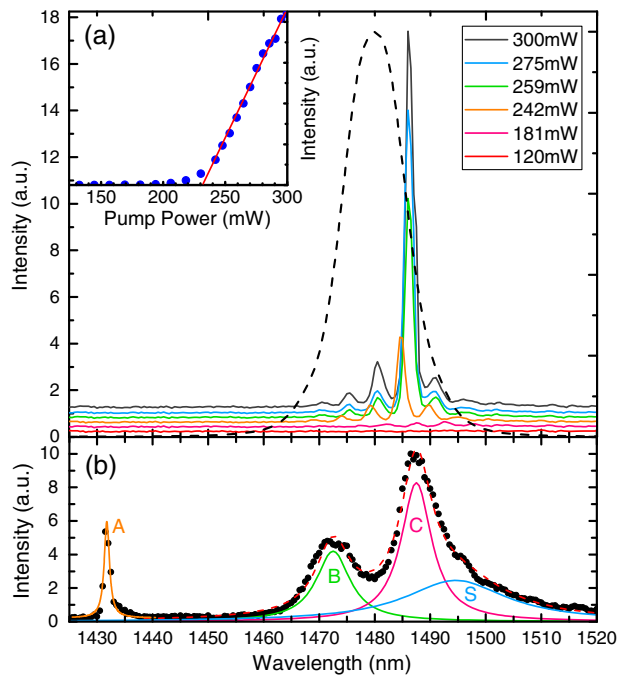
Fig. 1. (a) Emission spectrum observed at various pump powers (vertically shifted by 0.2 for readability). The black dashed curve depicts the transmission properties of the bandpass filter. The inset shows the input–output curve of the spectral peak at 1485 nm. (b) Spontaneous emission spectrum of a single hole array (other array gave identical results).
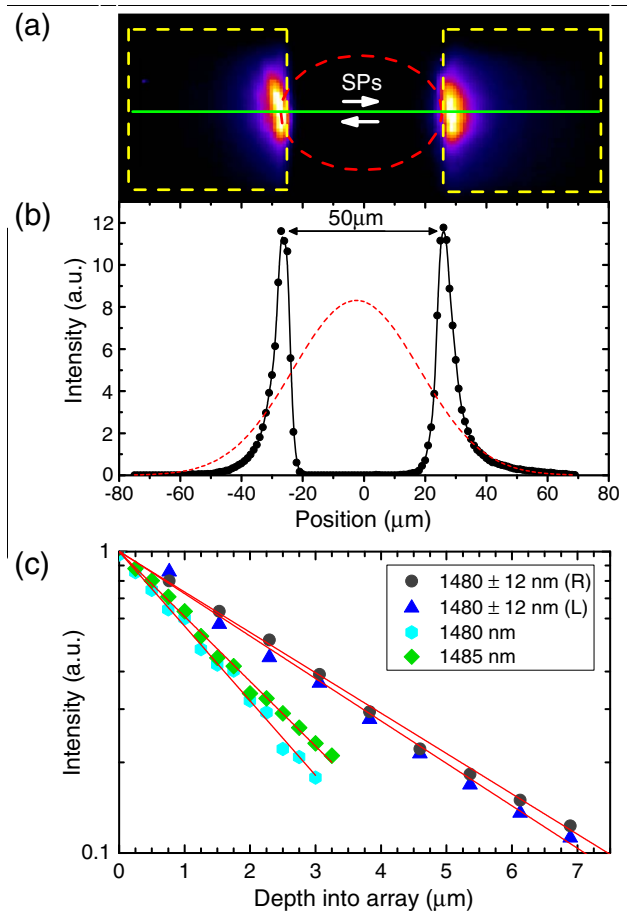

Fig. 2. (a) Direct image of the emission on the air side of the structure observed with the CCD. The yellow dashed lines indicate the edges of the two hole arrays. The red dashed line indicates the approximate pump shape at FWHM. (b) Intensity of emission (black) and excitation spot (red dashed) along the central green line in (a). (c) Log-plot of the intensity that shows the exponential decay into the arrays.

the same excitation spot. These numbers correspond to peak fluences of ≈ 100 and 90 kW/cm^2, respectively.

Figure 1(a) depicts the emission spectrum at various pump powers, as observed in the high-intensity region of the direct image. Above the lasing threshold, several spectral peaks, or lasing modes, become prominently visible. These peaks are spaced with a period of 5.2 ± 0.1 nm and gradually shift to higher wavelengths when the input power is increased. We will focus on the lasing modes at 1480 and 1485 nm and combine these results with CCD observations behind the aforementioned bandpass (BP) filter. For comparison, Fig. 1(b) shows that the spontaneous emission spectrum of an individual array comprises four modes (labeled A, B, C, and S as in [21]), which show up as Lorentzian resonances.

Figure 2(a) shows a direct image of the emission from the air side of the gold film, under excitation from the semiconductor side with a pump spot that covers both the central region and part of the hole arrays at $P_{\text{in}} = 300$ mW. The SP field intensity is expected to be most intense in the central region, but is hardly visible through the gold film.

Figure 2(b) shows the intensity along the central green line. An approximately exponential decay into the arrays is apparent and further confirmed by the log-plot in Fig. 2(c). Fits of these measurements yielded penetration depths $d_{\text{pen}}^L = 3.9 \pm 0.6$ µm and $d_{\text{pen}}^R = 3.2 \pm 0.5$ µm for the left and right arrays, respectively. Measurements with the scanning fiber, spectrally resolved at 1480 nm and 1485 nm, gave similar results of $d_{\text{pen}}^L = 2.3 \pm 0.3$ µm and $d_{\text{pen}}^R = 1.9 \pm 0.2$ µm. The measured penetration depth did not vary significantly with input power, both above and below lasing.

The far-field pattern observed by the CCD is depicted in Fig. 3. Coherent lasing emission from our effective double-slit geometry naturally leads to a Young's interference pattern in the far-field. The interference pattern has a fitted periodicity of 28 ± 2 mrad and a Lorentzian envelope with a width of 140 ± 5 mrad. This interference pattern was not visible below the lasing threshold.

We repeated this experiment with the scanning (multimode) fiber, for more spectral resolution, to find similar patterns with the same oscillation period and a slightly larger (~ 20 mrad) Lorentzian envelope (see black and red curves in Fig. 3 for cross sections). We also observed a 180° phase shift in the interference pattern at $\lambda = 1480$ nm, as compared to 1485 nm and BP-filtered measurements. The visibility of the oscillations increased when a single-mode fiber was used (at the expense of intensity).

The radiation pattern is modulated by a low-intensity dark band along $\theta_y \approx 0$ (see right-hand side of Fig. 3 for projected profile). This band was always present, but the profile's shape varied periodically with wavelength. As the wavelength increased from 1480 to 1485 nm, the two high-intensity peaks gradually moved inward and slowly lost intensity until at 1482.5 nm they both vanished at $\theta_y \approx 0$. Simultaneously, two new high-intensity peaks
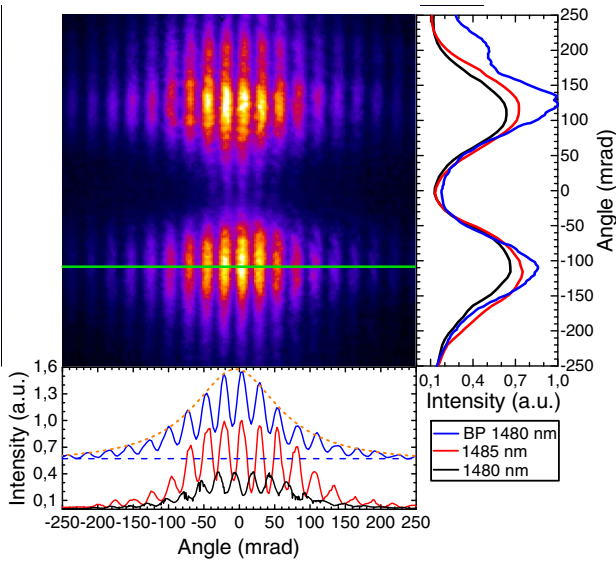
Fig. 3. Far-field (angular-resolved) emission from structure shown in Fig. 2. The intensity of the interference pattern along the horizontal green solid line is plotted in blue in the bottom figure (baseline shifted by 0.6). Spectrally resolved measurements at $\lambda = 1480$ nm (black) and 1485 nm (red) gave similar results. The right-hand figure shows the integrated intensity of the pattern along the horizontal axis.

moved in from wider angles and arrived at the same θ_y at the next lasing peak of 1485 nm.

Lasing action of our device is confirmed by three observations: the kink and steep linear increase in the input–output relation above the threshold of $P_{in} \approx 230$ mW, the spectral narrowing of the emitted light, and the observed far-field coherence.

The spectral peaks observed in Fig. 1(a) are the Fabry–Perot modes of the double-grating cavity. This assignment is confirmed by two observations. First, the 180° phase shift between the interference fringes observed for consecutive spectral modes (red and black curves in Fig. 3) agrees with the predicted change in symmetry of the EM field when the effective cavity length $m \cdot \lambda/2$ (for $m \in \mathbb{Z}$) changes from $m =$ even to $m =$ odd for consecutive longitudinal modes. Second, the measured wavelength difference of 5.2(1) nm is as expected for a Fabry–Perot cavity with a length of $L_{eff} = 50$ µm $+ d_{pen}^R + d_{pen}^L \approx 54$–57 µm. These numbers yield a group refractive index of $n_{group} = 3.82(11)$ for the circulating SPs, comparable to $n_{group} \approx 3.73$ calculated for $In_{0.53}Ga_{0.47}As$ around $\lambda \sim 1480$ nm at room temperature [22].

The spontaneous emission spectrum of a single hole array (1b) comprises four modes, labeled A, B, C, and S. These modes are linear combinations of the four $\pm x$ and $\pm y$ traveling SP waves that are combined and spectrally split by SP–SP scattering on the hole array [23]. Modes A and B are called "non-radiative," as their symmetry prevents emission along the surface normal, and modes C and S are "radiative." We only observe modes A and B as we also collect non-zero angles within our finite collection angle. Modes A, B, and C are TM polarized, whereas mode S is TE polarized. A comparison between Figs. 1(b) and 1(a) shows that the emission spectrum of our SP laser is positioned around the C mode of the individual arrays, with tails towards the B mode (mode S can be excluded on account of its different polarization). That lasing starts in the long-wavelength mode(s) instead of the

A mode is probably due to the asymmetry of the gain spectrum $g(\lambda)$, which is relatively broad and peaks at longer wavelengths [24]. That the double-grating laser operates close to the resonance frequencies of a single array is less obvious. As these resonances correspond to the "edges of the stopband" of a 2D DBR, the reflectivity $R(\lambda)$ of the 2D array will be larger in the center of the stopband. Still, the laser prefers to operate around the edge of the stopband.

The period of the far-field oscillations observed in Fig. 3 is Fourier related to the effective spacing between the two emitters via $\Delta\theta = \lambda_0/L_{eff}$, where the observed $\Delta\theta = 28(2)$ mrad corresponds to $L_{eff} = 53(3)$ µm. Likewise, the Lorentzian envelope in this figure (FWHM140 ± 5 mrad) provides an alternative estimate of the penetration depth via $d_{pen} = \lambda_0/(\pi \cdot \text{FWHM}) = 3.3(2)$ µm. This value agrees with results obtained from the direct images.

The intensity penetration depth provides information on the propagation and scattering of surface plasmons in the arrays [11,25,26]. The fitted d_{pen}^L was consistently ~20% larger than d_{pen}^R, suggesting higher in-plane scattering rates in the right array. This is as expected, as the production of the right array led to slightly larger hole sizes. That d_{pen} hardly varied with input power shows that the SP losses in our structure are dominated by scattering instead of absorption. We use a 1D DBR model to convert these penetration depths into the scattering rate γ (units s^{-1}) for incident SP plane waves on rows of holes [26]. The observed penetration depths correspond to a dimensionless scattering rate $\gamma/\omega_0 = a_0/(2\pi d_{pen}) = 0.018$–$0.038$ for the two arrays, where the equation is based on a simple rewrite from time to space domain. These numbers are somewhat larger than the values $\gamma/\omega_0 = 0.013$–0.017 [23] deduced from the observed SP dispersion in individual hole arrays with the same design. A natural reason for this difference is that the field penetration feels all scattering processes, whereas the value quoted for the dispersion measurements was for backscattering only. Additional scattering channels are the sideward scattering under $\pm 90°$ and the out-of-plane scattering of SPs to photons.

Finally, we discuss the dark band that is visible in the far-field pattern of Fig. 3. This dark band must originate from the 2D nature of the reflecting gratings, which makes this grating different from ordinary 1D DBRs. In single hole arrays, the symmetry of the non-radiative modes prevents emission along the surface normal and results in a donut-type lasing mode [15]. We expect similar effects for the backreflection of SPs in our second-order Bragg structure. We think the reason the projected intensity profile varies periodically with wavelength is as follows: the longitudinal wavevector of the SPs in the cavity is fixed by the round-trip condition between the arrays. The transverse wavevector is linked to the emission angles. Hence, larger emission angles correspond to larger total wavevectors and smaller emission wavelengths. This argument correctly predicts the periodicity and the sign (larger transverse angles for blue-detuned emission), making it a reasonable explanation.

In conclusion, we have observed an intriguing form of surface plasmon (SP) lasing, where the amplification occurs on a flat metal–dielectric interface with two hole arrays acting as 2D Bragg mirrors. This experiment provides a direct visualization of the propagation and scattering of SPs injected at the edge of a hole array. The observed penetration depth yields the scattering rate on rows of holes, and the lasing spectrum yields the SP group

velocity. Future challenges lay in the modeling of (i) the observed effective scattering rate and (ii) the nature of the dark band observed in the far-field interference pattern.

REFERENCES

1. H. Raether, *Surface Plasmons on Smooth and Rough Surfaces and on Gratings*, Vol. **111** of Springer Tracts in Modern Physics (Springer, 1988).
2. K. A. Willets and R. P. Van Duyne, Annu. Rev. Phys. Chem. **58**, 267 (2007).
3. J. N. Anker, W. P. Hall, O. Lyandres, N. C. Shah, J. Zhao, and R. P. Van Duyne, Nat. Mater. **7**, 442 (2008).
4. T.-F. Ma, Y.-P. Chen, J.-S. Guo, W. Wang, and F. Fang, TRAC Trends Anal. Chem. **103**, 102 (2018).
5. A. T. Reiner, S. Fossati, and J. Dostalek, Sens. Actuators B Chem. **257**, 594 (2018).
6. S. Lal, S. Link, and N. Halas, Nat. Photonics **1**, 641 (2007).
7. D. K. Gramotnev and S. I. Bozhevolnyi, Nat. Photonics **4**, 83 (2010).
8. P. Andrew and W. Barnes, Science **306**, 1002 (2004).
9. S. Bozhevolnyi, V. Volkov, E. Devaux, J.-Y. Laluet, and T. W. Ebbesen, Nature **440**, 508 (2006).
10. W. Wang, Q. Yang, F. Fan, H. Xu, and Z. L. Wang, Nano Lett. **11**, 1603 (2011).
11. W. L. Barnes, A. Dereux, and T. W. Ebbesen, Nature **424**, 824 (2003).
12. P. Mulvaney, Langmuir **12**, 788 (1996).
13. F. V. Beijnum, P. J. van Veldhoven, E. J. Geluk, G. W. 't Hooft, and M. P. van Exter, Appl. Phys. Lett. **104**, 061112 (2014).
14. I. De Leon and P. Berini, Nat. Photonics **4**, 382 (2010).
15. F. van Beijnum, P. J. van Veldhoven, E. J. Geluk, M. J. A. de Dood, G. W. 't Hooft, and M. P. van Exter, Phys. Rev. Lett. **110**, 206802 (2013).
16. M. A. Noginov, G. Zhu, M. Mayy, B. A. Ritzo, N. Noginova, and V. A. Podolskiy, Phys. Rev. Lett. **101**, 226806 (2008).
17. C. Zhang, Y. Lu, Y. Ni, M. Li, L. Mao, C. Liu, D. Zhang, H. Ming, and P. Wang, Nano Lett. **15**, 1382 (2015).
18. M. Noginov, G. Zhu, A. Belgrave, R. Bakker, V. Shalaev, E. Narimanov, S. Stout, E. Herz, T. Suteewong, and U. Wiesner, Nature **460**, 1110 (2009).
19. M. T. Hill, Y.-S. Oei, B. Smalbrugge, Y. Zhu, T. de Vries, P. J. van Veldhoven, F. W. M. van Otten, T. J. Eijkemans, J. P. Turkiewicz, H. de Waardt, E. J. Geluk, S.-H. Kwon, Y.-H. Lee, R. Nötzel, and M. K. Smit, Nat. Photonics **1**, 589 (2007).
20. R. F. Oulton, V. J. Sorger, T. Zentgraf, R.-M. Ma, C. Gladden, L. Dai, G. Bartal, and X. Zhang, Nature **461**, 629 (2009).
21. V. T. Tenner, M. J. A. de Dood, and M. P. van Exter, Opt. Express **24**, 29624 (2016).
22. S. Adachi, J. Appl. Phys. **66**, 6030 (1989).
23. M. P. van Exter, V. T. Tenner, F. Beijnum, M. J. A. de Dood, P. Veldhoven, E. J. Geluk, and G. W. 't Hooft, Opt. Express **21**, 27422 (2013).
24. K. Petermann, *Laser Diode Modulation and Noise* (Springer, 1991).
25. H. Ditlbacher, J. R. Krenn, G. Schider, A. Leitner, and F. R. Aussenegg, Appl. Phys. Lett. **81**, 1762 (2002).
26. H. A. Haus, *Waves and Fields in Optoelectronics* (Prentice-Hall, 1984).